

Article

Near-Infrared-Emitting *Meso*-Substituted Heptamethine Cyanine Dyes: From the Synthesis and Photophysics to Their Use in Bioimaging

Louise Kommers Reimann¹, Daniela de Souza Fortes¹, Fabiano da Silveira Santos¹, Henrique de Castro Silva Junior¹ , Ana Moira Morás², Dinara Jaqueline Moura², Rodrigo da Costa Duarte¹ and Fabiano Severo Rodembusch^{1,*} 

- ¹ Grupo de Pesquisa em Fotoquímica Orgânica Aplicada, Instituto de Química, Departamento de Química Orgânica, Universidade Federal do Rio Grande do Sul (UFRGS), Porto Alegre 91501-970, Brazil
² Laboratório de Genética Toxicológica, Universidade Federal de Ciências da Saúde de Porto Alegre (UFCSA), Porto Alegre 90240-511, Brazil
* Correspondence: fabiano.rodembusch@ufrgs.br

Abstract: Heptamethine cyanine dyes were synthesized in good yields by the reaction between quaternary indoles and a pentamethinic salt, under mild reaction conditions minimizing photooxidation. These compounds were used as precursors to prepare *meso*-substituted derivatives. The cyanine dye precursors presented UV-Vis absorption, related to fully allowed electronic transitions and fluorescence emission in the NIR region, without any evidence of aggregation in both ground and excited states. The substitution at the *meso* position showed a fundamental role in their photophysics, with the main absorption in the green-orange region related to the monomeric species. Moreover, the excited state photophysics presented emission profiles dependent on the excitation wavelengths, complicating the correlation of spectroscopy and structure. Density Functional Theory and OO-SCS-MP2 calculations under different solvation conditions revealed the heavy impact of conjugation effects on ground and excited states' geometries and electronic configurations of these compounds. Finally, the observed photophysical features of the *meso*-substituted heptamethine cyanine dyes were successfully used to explore their application as fluorescent probes in biological media, allowing stable staining in live and fixed cells.

Keywords: bioimaging; heptamethine cyanine; fluorescence; charge transfer; theoretical calculations



Citation: Reimann, L.K.; Fortes, D.d.S.; Santos, F.d.S.; Silva Junior, H.d.C.; Morás, A.M.; Moura, D.J.; Duarte, R.d.C.; Rodembusch, F.S. Near-Infrared-Emitting *Meso*-Substituted Heptamethine Cyanine Dyes: From the Synthesis and Photophysics to Their Use in Bioimaging. *Chemosensors* **2023**, *11*, 47. <https://doi.org/10.3390/chemosensors11010047>

Academic Editor: Pietro Salvo

Received: 13 December 2022

Revised: 31 December 2022

Accepted: 2 January 2023

Published: 5 January 2023



Copyright: © 2023 by the authors. Licensee MDPI, Basel, Switzerland. This article is an open access article distributed under the terms and conditions of the Creative Commons Attribution (CC BY) license (<https://creativecommons.org/licenses/by/4.0/>).

1. Introduction

Cyanines are a subclass of heterocyclic compounds ascribed as polymethine dyes presenting, in general, two heterocyclic moieties in their chemical structure where the bridges between them are π -conjugated systems. These compounds can be differentiated by the number of sp^2 carbons in the molecule central portion and the nature of the heterocyclic groups present in the peripheral molecular structure [1–4]. These structural changes allow large absorption intensities and spectral emissions ranging from ultraviolet to near-infrared regions [5–8]. Moreover, heptamethine cyanine dyes may be substituted at the *meso* position by reaction with nucleophilic compounds, such as amines, thiols, and aromatic or aliphatic alcohols [9–12]. In this regard, molecules presenting halogen atoms at the *meso* position provide a reactive site for this substitution in most cases, through a unimolecular radical nucleophilic substitution ($S_{RN}1$) mechanism, a substitution reaction in which a certain substituent on an aromatic compound is replaced by a nucleophile through an intermediary free radical species [13]. Additionally, cyanine dyes can be reactive to the environment, showing potential biomedical [14] and sensing applications [15,16], whereas the solvatochromic ones have been emerging mainly for analytical purposes [17]. Based on their electronic properties [18], they have been used as polarity sensors in several

studies related to halochromism [19], to study micro-heterogeneity in solution [20] and solvent mixtures [21]. In addition, heptamethine cyanine dyes have attracted attention for utilization in both imaging and therapy in cancer cells, mainly due to their low toxicity, accumulation capability, low autofluorescence, and superior signal-to-noise ratios [22–24]. A recent study showed that cyanine dyes efficiently labeled cancer cells and spontaneous tumors in transgenic mice, indicating their potential application to detect cancer metastasis and cancer cells in blood with a high degree of sensitivity [25].

Herein, we present the synthesis and photophysical characterization of new pyrrolidine-substituted heptamethine dyes, where the presence of the non-bonding electrons may be useful for different conjugation pathways where ICT may be present, and its preliminary investigation as fluorescent probes in biological media for cell staining.

2. Materials and Methods

2.1. Materials

2,3,3-Trimethylindolenine (CAS 1640-39-7), 1-iodomethane (CAS 74-88-4), 1-iodobutane (CAS 542-69-8), phosphorus(V) oxychloride (CAS 10025-87-3), 4-ethyl cyclohexanone (CAS 5441-51-0), triethylamine (CAS 121-44-8), hydrochloric acid (37%) (CAS 7647-01-0), aniline (CAS 62-53-3), and pyrrolidine (CAS 123-75-1) were purchased from Sigma-Aldrich (San Luis, MI, USA), and used as received. The syntheses were monitored by thin-layer chromatography using silica gel 60GF254 Merck (Darmstadt, Germany). The solvents acetonitrile (CAS 75-05-8), ethyl acetate (CAS 141-78-6), ethanol (CAS 67-63-0), toluene (CAS 108-88-3), dichloromethane (CAS 75-09-2), methanol (CAS 67-56-1), and hexane (CAS 110-54-3) were purchased from Honeywell (Charlotte, NC, USA), and used as received or purified according to the literature.

2.2. Characterization

Infrared absorption spectra were obtained on a Shimadzu-IR PRESTIGE-21 spectrometer on a KBr disc or operating on attenuated reflectance (ATR) mode, with a resolution of 4.0 cm^{-1} and 20 scans in the $4000\text{--}750\text{ cm}^{-1}$ range. Melting points were determined on a Fisatom 430D apparatus and are uncorrected. ^1H and ^{13}C NMR spectra were achieved on a Varian Inova operating at 300 or 400 MHz for ^1H and 75 or 100 MHz for ^{13}C , respectively, using deuterated solvents ($\text{DMSO-}d_6$ or CDCl_3). The chemical shifts (δ) are recorded in ppm and coupling constants (J) in Hz. ^1H NMR data have their data expressed as multiplicity (s, singlet; ls, large singlet; d, doublet; t, triplet; q, quintuplet; m, multiplet), coupling constant, and relative number of hydrogens. High-resolution mass spectra (HRMS-ESI) were recorded with electrospray ionization in the positive mode using a Bruker Impact II. The operating conditions were 4.5 kV for capillary voltage, and 33V and 2.5 V for sample and extraction cone voltage, respectively. Nitrogen was used as desolvation gas (N_2) to a temperature of $200\text{ }^\circ\text{C}$. Sodium formate was used for calibration. The original spectra from the spectroscopic characterization can be found as (Supplementary material Figures S1–S20). Spectroscopic grade solvents (Aldrich) were used for absorption in the Vis-NIR and fluorescence emission spectroscopies. All experiments were carried out at ambient room temperature ($25\text{ }^\circ\text{C}$) using solutions of concentrations between 10^{-5} and 10^{-6} M. The measurements were performed using $10 \times 10\text{ mm}$ path-length quartz cuvettes. Absorption spectroscopic measurements in the Vis-NIR region were obtained on a Shimadzu UV-2450 spectrometer. Fluorescence emission measurements were obtained on a Shimadzu RF-5301PC spectrofluorometer. The relative fluorescence quantum yields (Φ_{FL}) of the *meso*-substituted cyanines **8a–b** were obtained using cresyl violet in MeOH ($\Phi_{\text{FL}} = 0.54$) as a standard [26].

2.3. Synthesis

2.3.1. Indoles **3a–b**

To the reaction flask containing acetonitrile (10 mL), previously saturated for 15 min with nitrogen (N_2), the 2,3,3-trimethylindolenine **1** (1.9 mmol, 0.302 g) and the respective

1-iodoalkane (**2a** or **2b**) (9.9 mmol, 1.4 g for **2a** or 1.8 g for **2b**) were added under stirring. The reaction system was heated under reflux and nitrogen atmosphere for 6 h. After this period, the mixture was poured into 50 mL of ethyl acetate under stirring and heated for 30 min, after which time the supernatant was removed. This process was repeated 3 times. The obtained solids were filtered and dried at room temperature (25 °C). Indole **3a**: Pale yellow solid. Melting point: 240–242 °C. Yield: 72% (411 mg). ¹H NMR (DMSO-*d*₆, 300 MHz): δ (ppm) 7.91 (m, 1H); 7.82 (m, 1H); 7.60 (m, 2H); 3.97 (s, 3H); 2.78 (s, 3H); 1.52 (s, 6H). ¹³C NMR (DMSO-*d*₆, 75 MHz): δ (ppm) 196.4; 142.5; 142.0; 129.7; 129.2; 123.7; 115.6; 54.4; 35.3; 22.1; 14.9. Indole **3b**: Pale yellow solid. Melting point: (217–219 °C) [27]. Yield: 70% (456 mg). ¹H NMR (CDCl₃, 400 MHz): δ (ppm) 7.64 (m, 1H); 7.61 (m, 3H); 4.67 (t, 2H, J = 7.5 Hz); 3.13 (s, 3H); 1.96 (m, 2H); 1.67 (s, 6H); 1.53 (m, 2H); 1.01 (t, 3H, J = 6.0 Hz). ¹³C APT NMR (DMSO-*d*₆, 75 MHz): δ (ppm) 195.5; 141.5; 140.7; 130.0; 129.4; 123.4; 115.3; 54.6; 49.7; 29.8; 23.1; 20.0; 17.0; 13.6.

2.3.2. Pentamethine Salt **5** [28]

In an ice bath, phosphorus(V) oxychloride (22 mmol, 2.05 mL) was added dropwise in dimethylformamide (3 mL) and kept under stirring for 30 min. After this period, 4-ethyl cyclohexanone **4** (9.6 mmol, 1.35 mL) was added, and the temperature was increased up to reflux for 2 h. Then, the reaction was brought to room temperature (25 °C), an aniline/ethanol solution (6 mL) (1:1 *v/v*) was added, and the reaction was kept under stirring at room temperature for an additional 1 h. After this time, the reaction crude was poured into ice-cold H₂O and 20 mL of hydrochloric acid (37%) (10:1 *v/v*). The reaction was allowed to stand at room temperature for 12 h. Then, the solid was filtered, washed with H₂O, and recrystallized with toluene. The obtained solid was filtered, dried, and used for the next step without further purification. Pentamethine salt **5**: Violet solid. Melting point: (219–222 °C). Yield: 58% (2.15 g). FTIR (KBr, cm⁻¹): 3608, 3521, 3442, 3302, 2953, 2871, 1607, 1565, 1472. ¹H NMR (DMSO-*d*₆, 300 MHz): δ (ppm) 11.37 (ls, 2H); 8.51 (s, 2H); 7.60 (m, 4H); 7.44 (m, 4H); 7.25 (m, 2H); 3.07 (m, 2H); 2.18 (m, 2H); 1.65 (m, 1H); 1.47 (m, 2H, J = 7.2 Hz); 1.05 (t, 3H, J = 7.5 Hz).

2.3.3. Heptamethine Cyanine Dyes **6a-b**

In a round bottom amber flask containing acetonitrile (20 mL), previously dried and saturated for 15 min with nitrogen (N₂), the previously prepared pentamethine salt **5** (0.5 mmol, 0.193 g) was added under stirring and heated up to reflux temperature. In a second flask, acetonitrile (5 mL), triethylamine (1.5 mmol, 0.210 mL), and the respective indole (**3a** or **3b**) (1.5 mmol, 0.261 g for **3a** or 0.282 g for **3b**) were added and allowed to stir at room temperature (25 °C) for 5 min. After this time, the second flask solution was poured into the first one and then the reaction was allowed to stir at reflux temperature under a nitrogen atmosphere for a further 6 h. The reaction was checked for completion by TLC (dichloromethane/methanol 9:1, *v/v*). Finally, acetonitrile was evaporated on a rotatory evaporator and 2 mL of methanol was added to the reaction crude. Then, the reaction crude was poured into a solution of 100 mL of ethyl acetate/hexane (1:1 *v/v*) and placed in an ultrasonic bath for 30 min. After 12 h of solid decantation, the solid was filtered. This process was repeated 4 times. The final solids (**6a-b**) were filtered and dried. Heptamethine cyanine dye **6a**: Green solid. Melting point: (222–223 °C). Yield: 62% (190 mg). FTIR (KBr, cm⁻¹): 3603, 3521, 3326, 2962, 1651, 1551, 1365. ¹H NMR (CDCl₃, 300 MHz): δ (ppm) 8.34 (d, 2H, J = 12.0 Hz); 7.38 (m, 4H); 7.22 (m, 4H); 6.15 (d, 2H, J = 12.0 Hz); 3.73 (s, 6H); 2.88 (m, 2H); 2.24 (m, 2H); 1.71 (s, 12H); 1.57 (m, 2H); 1.05 (t, 3H, J = 7.5 Hz). ¹³C NMR (CDCl₃, 75 MHz): δ (ppm) 172.9; 150.7; 144.5; 142.7; 140.8; 128.8; 127.0; 125.3; 122.1; 110.9; 101.3; 49.2; 33.6; 32.6; 28.2; 28.0; 11.8. Heptamethine cyanine dye **6b**: Green solid. Melting point: 227–228 °C. Yield: 60% (210 mg). FTIR (KBr, cm⁻¹): 3517, 3330, 2957, 2862, 1665, 1556, 1514, 1428. ¹H NMR (CDCl₃, 400 MHz): δ (ppm) 8.36 (d, 2H, J = 16.0 Hz); 7.41 (m, 4H); 7.29 (m, 2H); 7.21 (m, 2H); 6.20 (d, 2H, J = 12.0 Hz); 4.21 (t, 2H, J = 8.0 Hz); 2.90 (m, 2H); 2.27 (m, 2H); 1.74 (s, 12H); 1.68 (m, 1H); 1.61 (m, 2H); 1.51 (q, 2H; J = 8.0 Hz); 1.04 (m, 9H).

^{13}C NMR (CDCl_3 , 100 MHz): δ (ppm) 172.4; 150.4; 144.4; 142.1; 141.0; 128.8; 126.5; 125.4; 122.3; 111.0; 101.1; 49.4; 44.8; 33.6; 32.0; 29.4; 28.1; 20.3; 13.8; 11.7.

2.3.4. *Meso*-Substituted Heptamethine Cyanine Dyes **8a-b**

In a round bottom amber flask containing acetonitrile (2 mL), previously dried and saturated for 15 min with nitrogen (N_2), the respective cyanine **6a** (7.80×10^{-2} mmol, 0.05 g) or **6b** (7.80×10^{-2} mmol, 0.05 g) was added under stirring. To this solution, pyrrolidine **7** (24.4 mmol, 1.5 mL) was added. The reaction was allowed to stir at reflux temperature under a nitrogen atmosphere for a further 30 min. The reaction was followed by thin-layer chromatography (TLC) using dichloromethane/ethyl acetate/methanol (45:45:10 *v/v/v*) as eluent. After completion of the reaction, the mixture was evaporated to dryness. The resulting crude residue was purified by column chromatography over silica gel and using the same mixture used for TLC as eluent to afford the derivatives **8a-b**. *Meso*-substituted heptamethine cyanine dye **8a**: violet solid. Melting point: 95–98 °C. Yield: 78% (39 mg). FTIR (KBr, cm^{-1}): 3387, 2955, 2917, 2854, 1538, 1305, 1187, 794. ^1H NMR ($\text{DMSO-}d_6$, 300 MHz): δ (ppm) 7.39 (d, 2H, $J = 6.0$ Hz); 7.25 (t, 2H, $J = 9.0$ Hz); 7.16 (d, 2H, $J = 12.0$ Hz); 7.03 (d, 2H, $J = 6.0$ Hz); 6.97 (t, 2H, $J = 9.0$ Hz); 5.44 (d, 2H, $J = 6.0$ Hz); 4.04 (m, 4H); 3.33 (s, 6H); 2.80 (d, 2H, $J = 15.0$ Hz); 2.17 (m); 2.0 (m, 4H); 1.57 (s, 6H); 1.54 (s, 6H); 1.46 (m, 2H); 1.02 (t, 3H, $J = 9.0$ Hz). ^{13}C NMR ($\text{DMSO-}d_6$, 75 MHz): δ (ppm) 173.5; 164.3; 144.4; 139.5; 133.9; 128.4; 122.3; 121.6; 121.1; 108.3; 92.2; 55.5; 46.6; 34.2; 29.6; 28.6; 28.2; 24.2; 12.2. HRMS (ESI-qTOF) m/z : $[\text{M} + \text{H}]^+$ calculated for $\text{C}_{38}\text{H}_{48}\text{N}_3$: 546.3841; found 546.3843. *Meso*-substituted heptamethine cyanine dye **8b**: violet solid. Melting point: 114–115 °C. Yield: 75% (38 mg). FTIR (KBr, cm^{-1}): 3401, 2952, 2918, 2861, 1541, 1187, 1102, 739. ^1H NMR ($\text{DMSO-}d_6$, 400 MHz): δ (ppm) 7.36 (d, 2H, $J = 8.0$ Hz), 7.21 (m), 7.13 (d, 2H, $J = 12.0$ Hz), 6.99 (d, 2H, $J = 8.0$ Hz), 6.94 (t, 2H, $J = 4.0$ Hz), 5.46 (d, 2H, $J = 12.0$ Hz), 4.02 (m, 4H), 3.82 (m), 2.75 (d, 2H, $J = 16.0$ Hz), 2.14 (m), 1.98 (m, 4H), 1.62 (m, 5H), 1.54 (s, 6H), 1.50 (s, 6H), 1.42 (m, 2H), 1.35 (m, 4H), 0.97 (t, 3H, $J = 8.0$ Hz), 0.92 (t, 6H, $J = 8.0$ Hz). ^{13}C NMR ($\text{DMSO-}d_6$, 100 MHz): δ (ppm) 172.9; 162.9; 143.4; 139.1; 133.5; 127.9; 121.9; 121.1; 120.4; 107.9; 91.7; 55.1; 46.2; 33.7; 33.5; 29.2; 27.9; 27.6; 23.7; 19.6; 13.7; 11.6. HRMS (ESI-qTOF) m/z : $[\text{M} + \text{H}]^+$ calculated for $\text{C}_{44}\text{H}_{60}\text{N}_3$: 630.4771; found 630.4782.

2.4. Theoretical Calculations

All DFT and ab initio calculations were performed using the ORCA v5.0.2 quantum chemistry package [29]. Initial geometries for heptamethine cyanine dyes **6a** and **8a** were obtained after conformational sampling using the CREST software [30]. This procedure was, in turn, based on energies obtained by the accurate semi-empirical method GFN2-xTB [31]. The lowest conformers were subsequently optimized to the ground (GS) and first excited states (ES) using Density Functional Theory via the B97-3c scheme [32], which is a revamped version of Becke's B97 GGA functional [33], with a slightly modified version of the triple- ζ Def2-TZVP basis set [34] and including the D3 dispersion correction [35] and a Short-Range Basis (SRB) correction [36]. We used an improved version of the Conductor-like Continuum Polarization Model called LR-CPCM to simulate solvent relaxation during geometric optimizations to the ground and excited states [37]. A better description of charge transfers and energy gaps was achieved on a higher OO-SCS-MP2/Def2-TZVP computational level as properties dependent on virtual orbitals are not always correctly described by the DFT method [38]. All calculations were set to tight convergence criteria of $1.0\text{E-}08$ a.u with isosurfaces using $\rho = 0.05$ $\text{e}/\text{\AA}^3$ and 3D molecular representations using the CPK color scheme.

2.5. Cellular Stain

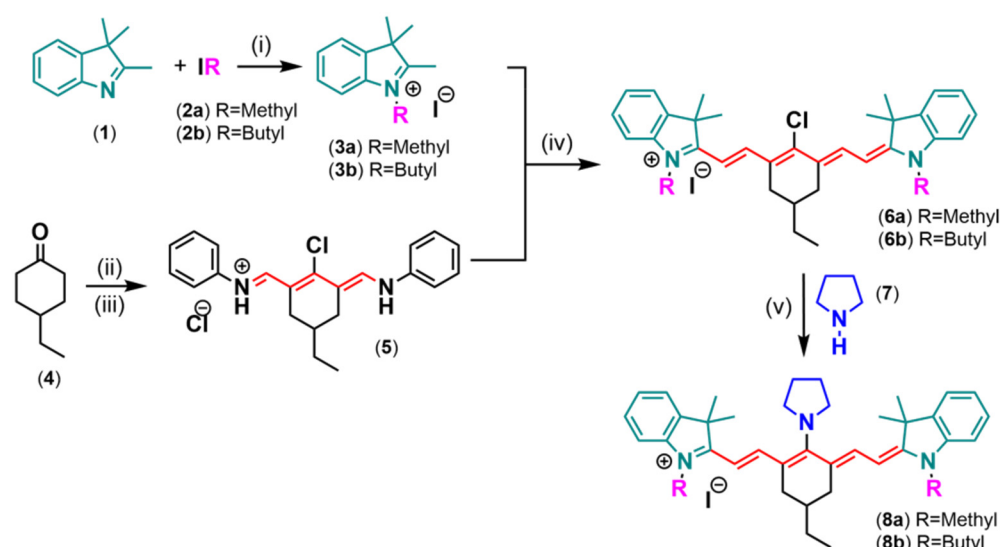
The glioblastoma multiform T89G cells were acquired by American Type Culture Collection[®] (ATCC). The cells were grown in Dulbecco's modified Eagle's medium (Gibco[™] DMEM, Life Technology, Grand Island, NY, USA) supplemented with 10% heat-inactivated fetal bovine serum (Gibco[™] FBS, Life Technology, Grand Island, NY, USA), 100 units- mL^{-1} of

penicillin, and $100 \text{ g}\cdot\text{mL}^{-1}$ of streptomycin at 37°C in a humidified atmosphere with 5% CO_2 . To investigate the fluorescence stain capacity of the studied heptamethine cyanine dyes, cells grown on 96-well plates were fixed in paraformaldehyde (4%), washed with PBS, and permeabilized in Triton X-100 (0.01%). The stock solutions of the cyanine dyes were solubilized in ethanol at $5 \mu\text{M}$. All solutions were vortexed for 1 min and sonicated for 30 min. The cells were then washed with PBS and incubated with the cyanine dyes chosen as the model, in stock solutions concentrations (30 min, 37°C). Nuclei were contrasted with Hoechst ($4 \mu\text{g}\cdot\text{mL}^{-1}$ for 10 min). Finally, the cells were imaged in INCell analyzer 2200 (GE Healthcare Life Sciences, Piscataway, NJ, USA) after 30 min and 24 h of staining. To investigate the fluorescence stain capacity in non-fixed samples, cells grown on 96-well plates were washed with PBS and incubated with the studied cyanine dyes in stock solution concentrations (30 min, 37°C). Nuclei were contrasted with Hoechst ($4 \mu\text{g}\cdot\text{mL}^{-1}$ for 10 min). Finally, the cells were imaged in an INCell analyzer 2200 (GE Healthcare Life Sciences, Piscataway, NJ, USA). To verify if there was a loss of confluence after treatment with cyanine dye **8a**, T98G cells were grown in a 96-well plate and incubated with increasing concentrations of the compound ($0.005\text{--}5 \mu\text{M}$) and, after 30 min, photos were acquired with an increase of 5x in an inverted optical microscope (TCM400, Labo America, Fremont, CA, USA).

3. Results and Discussion

3.1. Synthesis

The heptamethine cyanine dyes **6a-b** were prepared as presented in Scheme 1. The quaternary indoles **3a-b** were synthesized in previously dried, and N_2 -saturated acetonitrile using an excess of the respective alkyl halides **2a-b** [39]. It is worth mentioning that in this reaction, the protection from light and the N_2 atmosphere played an important role in this reaction [40]. The heptamethine cyanine dyes **6a-b** were synthesized by the reaction between the quaternary indoles **3a-b** and the pentamethine salt **5** [41–43]. The reaction was performed protected from light in amber round bottom flasks to minimize their photooxidation [43]. HPLC-grade solvents were previously saturated with N_2 for at least 20 min, and the reaction took place under an N_2 atmosphere during the heating step. These procedures allowed for obtaining the reaction crude presenting only the characteristics of the desired products, suggesting the importance of reducing the photooxidation process during the reaction. It is important to note that the order of substrate addition played a fundamental role in cyanine synthesis. Using the following sequence: pentamethine salt **5**, indole **3a-b**, and triethylamine, the reaction medium, which is predominantly red due to the high molar absorptivity of the pentamethine salt, turns yellow, and the conversion of reagents is affected after 24 h of reaction. To prove that the yellow color arises from the deprotonated compound **5**, triethylamine was added dropwise into an acetonitrile solution of **5**. The observed behavior was similar to that expected, where the reaction media became yellow. This result indicates that the pentamethine salt presents higher reactivity in the protonated specie as the literature reports reaction yields between 32 and 45% using pyridine as the solvent [44]. Finally, the *meso*-substituted heptamethine cyanine dyes **8a-b** were prepared as also presented in Scheme 1. In this reaction, an $\text{S}_{\text{RN}}1$ mechanism is believed to be present in the presence of aprotic polar solvents, such as dimethylformamide, dimethylsulfoxide, and acetonitrile [13].



Scheme 1. Synthesis of heptamethine cyanine dyes **6a-b** and the respective *meso*-substituted derivatives **8a-b**: (i) acetonitrile, N₂, reflux, 6 h; (ii) POCl₃/dimethylformamide, reflux 2 h; (iii) aniline/ethanol, 1h, H₂O/HCl, r.t. 15 h; (iv) acetonitrile, triethylamine, reflux, 6 h; (v) acetonitrile, N₂, reflux, 30 min.

3.2. Photophysical Characterization

The photophysical study in solution was performed using organic solvents with different dielectric constants (ethyl acetate, dichloromethane, methanol, and acetonitrile). The relevant data from the steady-state ground and excited states characterization are summarized in Table 1. Figure 1 presents the UV-Vis absorption and fluorescence emission spectra of the heptamethine cyanine dye **6a**, which was chosen as a representative structure of the synthesized cyanine precursor. It is worth mentioning that the cyanine dye **6b** presented absorption and emission curves with similar shapes and absorption maxima locations (Figure S21).

Table 1. Photophysical data of heptamethine cyanine dyes **6a-b** in solution, where λ_{abs} and λ_{em} are the absorption and emission maxima (nm), respectively; ϵ is the molar extinction coefficient ($\text{M}^{-1}\cdot\text{cm}^{-1}$); f_e is the calculated oscillator strength; k_e^0 is the calculated radiative rate constant ($\times 10^8 \text{ s}^{-1}$); τ^0 is the calculated pure radiative lifetime (ns); $\Delta\lambda_{\text{ST}}$ is the Stokes shift (nm/cm^{-1}); E_g is the optical bandgap (eV).

Cyanine	Solvent	λ_{abs}	ϵ	f_e	k_e^0	τ^0	E_g	λ_{em}	$\Delta\lambda_{\text{ST}}$
6a	Ethyl acetate	778	197,000	0.303	0.50	1.998	1.49	785	7/115
	Dichloromethane	789	288,000	0.345	0.55	1.806	1.49	790	1/16
	Methanol	774	205,000	0.289	0.48	2.075	1.48	782	8/132
	Acetonitrile	775	225,000	0.329	0.55	1.826	1.50	787	12/197
6b	Ethyl acetate	783	189,000	0.249	0.41	2.465	1.48	784	1/16
	Dichloromethane	789	206,000	0.217	0.35	2.864	1.48	793	4/64
	Methanol	780	365,000	0.445	0.73	1.367	1.48	784	4/65
	Acetonitrile	780	284,000	0.330	0.54	1.845	1.49	792	12/194

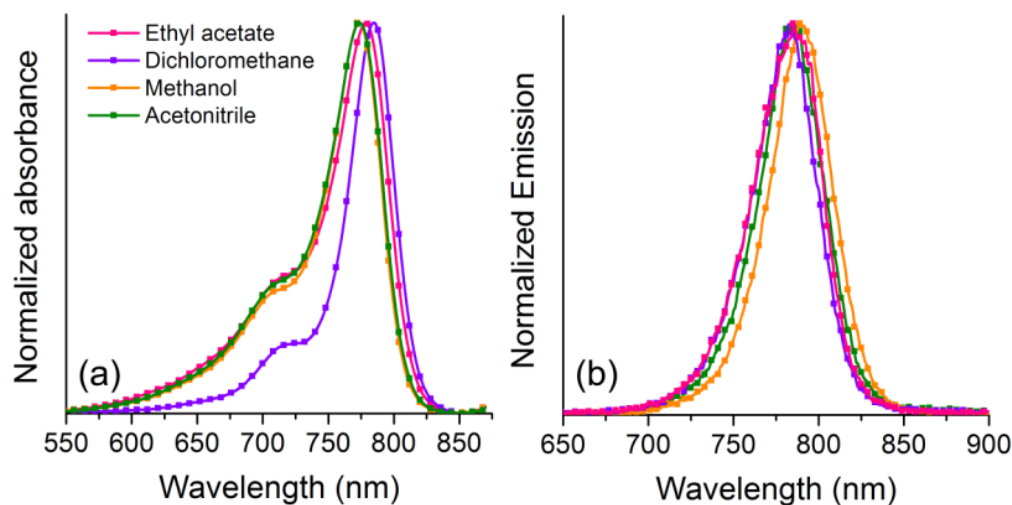


Figure 1. (a) UV-Vis absorption and (b) steady-state fluorescence emission spectra in solution of different organic solvents ($\sim 10^{-6}$ M) of the heptamethine cyanine dye **6a**.

The heptamethine cyanine dye **6a** presents absorption maxima in the NIR region, between 774 and 789 nm, depending on the solvent polarity with no clear tendency on the environment polarity. It could be observed that the cyanine dyes presented an absorption maxima variation ($\Delta\lambda_{\text{abs}}$) of 14 nm/229 cm^{-1} (**6a**) and 9 nm/146 cm^{-1} (**6b**), which can be related to cyanine-type electronic transitions, as already observed in similar compounds [9]. In this evaluation, methanol was excluded due to its specific interactions with the compounds. In addition, the UV-Vis spectra plotted in epsilon value showed similar intensities (Figure S22), which exclude a possible ion-pairing effect that may occur in the less polar environment, especially considering an iodine counterion [45]. The photophysical investigation in the ground state also allowed for obtaining the experimental extinction coefficient (ϵ) and, from the Strickler–Berg relations (Equations (1) and (2)), the theoretical rate constant for emission (k_e^0) and the respective oscillator strengths (f_e) [46]:

$$f_e \approx 4.3 \times 10^{-9} \int \epsilon d\bar{\nu} \quad (1)$$

$$k_e^0 \approx 2.88 \times 10^{-9} \bar{\nu}_0^0 \int \epsilon d\bar{\nu} \quad (2)$$

For an electronic transition, the respective oscillator strength can be obtained from Equation (1), which relates the area under the absorption curve from a plot of the molar absorptivity coefficient ϵ ($\text{M}^{-1} \cdot \text{cm}^{-1}$) against wavenumber $\bar{\nu}$ (cm^{-1}). The same integral, applying Equation (2), allows the obtention of the theoretical rate constant for emission (k_e^0) (Equation (2), where the definition of $\bar{\nu}_0^0$ is the wavenumber (energy in $1/\lambda$ units) of the absorption band maximum). In addition, from the k_e^0 , the pure radiative lifetime τ^0 can be obtained, defined as $1/k_e^0$ [47]. The high molar absorptivity coefficient values ($\epsilon \sim 10^5 \text{ cm}^{-1} \cdot \text{M}^{-1}$), as well as the respective calculated radiative rate constants (k_e^0), indicate, for all studied compounds, spin- and symmetry-allowed electronic transitions, which could be related to ${}^1\pi\text{-}\pi^*$ transitions (Table 1). It could also be observed in methanol that these cyanines presented an increase in the molar absorptivity coefficient value, increasing the alkyl chain of the indolic ring, as already reported in the literature [41]. The observed electronic transitions are associated with a small optical bandgap between the HOMO and LUMO orbitals (~ 1.5 eV) as already reported for different chromophores absorbing in the NIR region [48,49]. Moreover, such transitions are related to non-aggregated species, so-called monomeric ones [50]. In this sense, it is worth mentioning that the studied heptamethine cyanine dyes presented shoulder-like blue-shifted absorption, located around 720 nm, which is usually reported in the literature as an electronic transition related to the

formation of H-type aggregates [51,52]. To clarify this topic, fluorescence emission spectra of these compounds were acquired at different concentrations and excitation wavelengths, including 720 nm. In addition, their respective excitation spectra were also obtained (Figures S23–S27). These results indicate that the observed blue-shifted bands are probably related to vibronic structure. In addition, an almost constant radiative lifetime τ^0 suggests that after the radiation absorption, the heptamethine cyanine dyes populate the same excited state. Figure 1b depicts the fluorescence emission spectra, obtained by exciting the compounds at the absorption maxima (Table 1). In general, these compounds present a relatively sharp emission between 700 and 850 nm, with a small Stokes shift (up to 12 nm/197 cm^{-1}), which is characteristic for this class of molecules, showing almost absent differences between the electronic structure of the ground and excited states.

The photophysical study in solution was also performed for the *meso*-substituted heptamethine cyanine dyes **8a-b**. The relevant data from the steady-state ground and excited states characterization are summarized in Table 2. The fluorescence emission spectra were obtained by exciting the compounds at the absorption located between 559 and 611 nm (Table 2). Figure 2 shows the absorption of cyanine dye **8a** (Figure 2a) and **8b** (Figure 2b), as well as a concentration study of compound **8b** in acetonitrile.

Table 2. Photophysical data of heptamethine cyanine dyes **8a-b** in solution, where λ_{abs} is the absorption maximum (nm), ϵ is the molar extinction coefficient ($\text{M}^{-1}\cdot\text{cm}^{-1}$), f_e is the calculated oscillator strength, k_e^0k is the calculated radiative rate constant ($\times 10^8 \text{ s}^{-1}$), and τ^0 is the calculated pure radiative lifetime (ns).

Cyanine	Solvent	λ_{abs}	ϵ	f_e	k_e^0k	τ^0
8a	Dichloromethane	602	47,400	0.578	1.60	0.627
	Ethanol	578	41,900	0.622	1.86	0.537
	Methanol	572	42,900	0.578	1.77	0.566
	Acetonitrile	559	36,000	0.525	1.68	0.595
8b	Dichloromethane	611	65,300	0.728	1.95	0.513
	Ethanol	587	55,600	0.753	2.19	0.458
	Methanol	581	43,000	0.618	1.83	0.546
	Acetonitrile	570	46,000	0.626	1.93	0.519

It can be observed that both cyanines present absorption in the visible region, with any significant dependence on the alkyl chain. In addition, the main absorption bands shift to lower wavelengths (559–611 nm) if compared to the cyanine precursors **6a-b** (~780 nm), as well as present a more significant solvatochromism (43 nm for **8a** and 41 nm for **8b**). Although it does not present a clear tendency, this latter seems to present a negative solvatochromic effect, indicating a higher dipole moment in the ground state. All these features indicate a loss of cyanine character, allowed by the substitution at the *meso* position of the cyanine [10]. In this case, the change of the chlorine atom by pyrrolidine seems to increase the electron-donating ability of the central substituent, allowing a progressive localization of the positive charge on the central carbon atom of the polymethine chain. Thus, the charge delocalization on the π -conjugated structure is reduced, and the cyanine character is lost. Instead, a bis-dipole structure is reached, described as a central cationic acceptor bearing two electron-donating moieties [53]. In addition, by applying the Strickler–Berg relations, the main electronic transitions could be related to fully allowed transitions, related to π – π^* (Table 2). It is worth mentioning that these derivatives presented additional absorption bands located around 450 nm, as already observed in the literature for similar compounds [11]. As already discussed for precursors **6a-b**, it is believed that these bands arise from the monomeric species, being related to vibronic structures of the cyanines and not from H-aggregates, as usually reported in the literature [54]. Finally, an additional red-shifted absorption band located around 700 nm was already observed [11], which is absent in the cyanine precursors. The correlation between J-aggregates and this absorption band located at longer wavelengths was discarded as it is well-known that these aggregates

present quite particular features. The absorption maxima shift to longer wavelengths (~ 100 nm) with a dramatic sharpening in width (10–20 nm) [55], and a strong increase in the molar absorbance in comparison with isolated monomers [56]. These aggregates are concentration-dependent, a behavior that was not observed in the studied cyanine dye **8b** in acetonitrile (Figure 2c). For the concentration study, similar results were found in dichloromethane, 1,4-dioxane, and ethanol (Figures S28 and S29). Additional experiments were also performed as already discussed in the literature to induce the aggregation in these compounds [57], without any clear indication of its formation (Figures S31 and S32), which corroborates with the affirmation that all observed absorption bands are related to their monomeric species. Although the excited state investigation concerning heptamethinecyanines is less studied if compared to the UV-Vis data, probably due to its particular photophysics, some studies can be found and are related to the presence of monomeric species in solution or even aggregates [58]. In this way, aiming to bring some light to this discussion and based on the ground state results obtained in this investigation, the steady-state fluorescence emission was performed with cyanine dyes **8a-b**. In this sense, PL spectra were obtained at different excitation wavelengths (Figure 3a,b). The relevant data from this investigation are summarized in Table 3. It is worth mentioning that the emission spectra of cyanine dye **8a** presented the same emission profile (Figures S33 and S34). It can be observed that cyanine dye **8b** after excitation between 581 and 611 nm presents in all studied solvents a dual fluorescence emission located around 650 and 750 nm. The main emission in dichloromethane and polar protic media is located at higher energies, and in acetonitrile, the emission band is located at longer wavelengths (Figure 3a). However, under excitation between 708 and 715 nm, the main fluorescence emission can be observed located around 725 nm (Figure 3b). Based on the ground and excited state photophysics, the observed emission profiles seem not to be related to aggregation in solution [58]. In addition, relatively large Stokes shift values ($3329\text{--}4868\text{ cm}^{-1}$) could be calculated for the synthesized compounds under excitation between 581 and 611 nm, as shown in Table 3. Usually, this parameter is polarity dependent, as observed in this study, where more polar solvents presented higher Stokes shift values. This behavior indicates that different electronic structures are present between the ground and the excited states, as reported in the literature for similar compounds [18]. Thus, it is believed that the observed dual fluorescence emission with a large Stokes shift may be evidence of intramolecular charge transfer (ICT) between electron donor and acceptor groups present in the molecular structure [18]. In this way, as observed in Figure 3a, the emission profiles can be related to both locally excited (blue-shifted, Stokes shift $\sim 1500\text{ cm}^{-1}$) and charge transfer (red-shifted, Stokes shift $\sim 4000\text{ cm}^{-1}$) species. The fluorescence quantum yield values were measured from emission curves obtained using the absorption maxima as excitation wavelengths, and the values are in agreement with the literature [11].

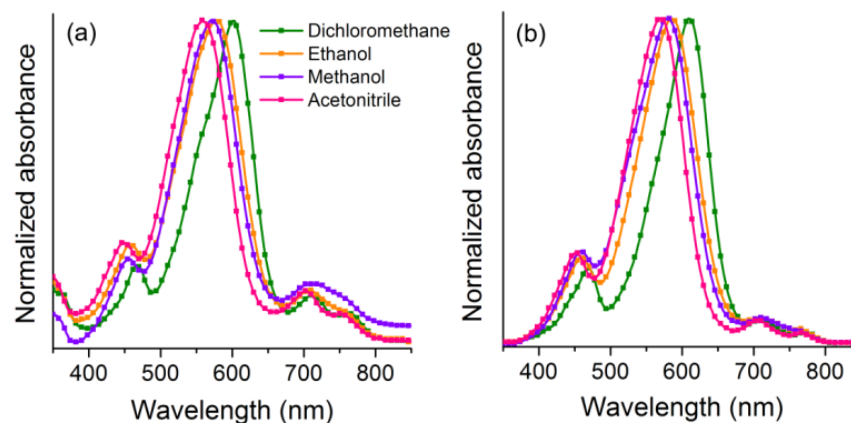


Figure 2. Cont.

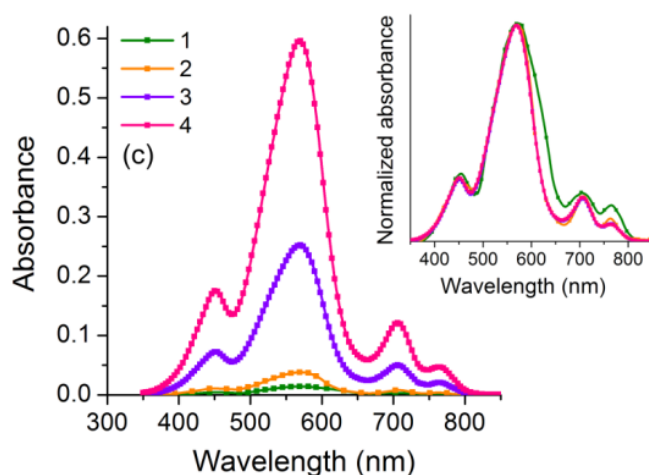


Figure 2. Normalized UV-Vis absorption spectra of heptamethine cyanine dyes (a) **8a** and (b) **8b** in a solution of different organic solvents ($\sim 10^{-6}$ M) and (c) cyanine dye **8b** in acetonitrile at different concentrations ($1: 5.0 \times 10^{-7}$ M, $2: 1.0 \times 10^{-6}$ M, $3: 5.0 \times 10^{-6}$ M, and $4: 5.0 \times 10^{-5}$ M). The inset shows the respective normalized UV-Vis spectra. (DCM = dichloromethane).

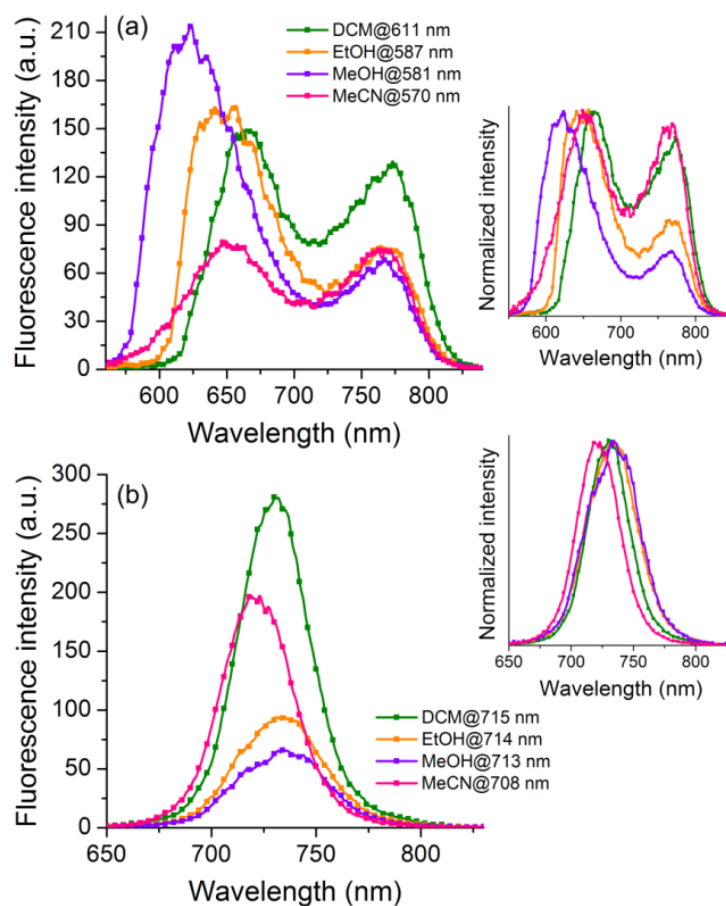


Figure 3. Steady-state fluorescence emission spectra of heptamethine cyanine dye **8b** in a solution of different organic solvents ($\sim 10^{-6}$ M) at excitation wavelength between (a) 581 and 611 nm (Table 2) and (b) 708 and 715 nm (Table S2). The inset shows the respective normalized spectra. (DCM = dichloromethane, MeCN = acetonitrile and MeOH = methanol).

Table 3. Excited-state photophysical data of *meso*-substituted heptamethine cyanine dyes **8a–b** in solution, where λ_{em} is the emission maximum (nm) at different excitation wavelengths (λ_{exc} in nm), $\Delta\lambda_{ST}$ is the Stokes shift (cm^{-1}), and Φ_{FL} is the fluorescence quantum yield.

Cyanine	Solvent	λ_{exc} ^(a)	LE		ICT		λ_{exc} ^(b)	LE		ICT		Φ_{FL}
			λ_{em}	$\Delta\lambda_{ST}$	λ_{em}	$\Delta\lambda_{ST}$		λ_{em}	$\Delta\lambda_{ST}$	λ_{em}	$\Delta\lambda_{ST}$	
8a	Dichloromethane	602	666	1596	774	3691	712	731	365	-	-	0.25
	Ethanol	578	647	1845	769	4297	708	735	519	-	-	0.16
	Methanol	572	624	1457	768	4462	703	736	638	-	-	0.32
	Acetonitrile	559	652	2552	768	4868	712	721	175	-	-	0.17
8b	Dichloromethane	611	660	1215	767	3329	715	727	231	-	-	0.27
	Ethanol	587	654	1745	764	3947	714	729	288	-	-	0.25
	Methanol	581	647	1756	763	4106	713	732	364	-	-	0.32
	Acetonitrile	570	641	1943	763	4438	708	718	197	-	-	0.25

^(a) obtained from the absorption spectra (maxima). ^(b) obtained from the absorption spectra (redshifted bands).

On the other hand, due to the single fluorescence emission with a small Stokes shift ($\sim 500 \text{ cm}^{-1}$), the observed emission in Figure 3b seems to arise from a locally excited specie. To better understand the observed photophysics, the difference in the dipole moments between the excited and ground states was obtained for cyanine dye **8b** by applying the simplified Lippert–Mataga correlation presented in Equation (3) [59], where h is Planck’s constant, c is the speed of light, a is the Onsager cavity radius, and μ_g and μ_e are the dipole moments of the solute in the ground and excited states, respectively. In this plot, a linear relation of the absorbance or fluorescence maxima versus the solvent polarity function can be related to the internal charge transfer character [60,61]. The relevant data from this investigation are summarized in Table S1. Macroscopically, Equation (3) relates solvatochromic shifts from the Stokes shift versus the orientation polarization function (Δf). This latter is given by Equation (4) [47], where ϵ and n are the dielectric constant and the refractive index, respectively, for a mixture of solvents (Equations (5) and (6)) [62]. In this mixture, f_A and f_B are the volumetric fractions of the two solvents.

$$\Delta\bar{\nu}_{st} = \frac{2(\mu_e - \mu_g)^2}{hca^3} \Delta f + \Delta\bar{\nu}_0 \quad (3)$$

$$\Delta f = \frac{(\epsilon - 1)}{(2\epsilon + 1)} - \frac{(n^2 - 1)}{(2n^2 + 1)} \quad (4)$$

$$\epsilon_{mix} = f_A \cdot \epsilon_A + f_B \cdot \epsilon_B \quad (5)$$

$$n_{mix}^2 = f_A n_A^2 + f_B n_B^2 \quad (6)$$

Figure 4 presents the Lippert–Mataga relationship between the absorption or emission maxima, as well as the Stokes shift. It is worth mentioning that this investigation was focused on the locally excited and intramolecular charge transfer emissions (see Figure 3a). The linear relationship between the absorption maxima with increasing solvent polarity (Figure 4a) and the upward curvature indicates that cyanine dye **8b** seems to be significantly destabilized in a more polar environment [63]. Taking the two emission bands into account (Figure 4b), a similar feature can be observed, once again with a positive slope with the solvent polarity function Δf . These results indicate that despite quaternary nitrogen in the indolic moiety, this compound seems to present low polarity in both ground and excited states. This latter can be related to a very effective delocalization of the positive charge into the cyanine skeleton. Surprisingly, the emission bands also seem to be equally affected by the solvent polarity (Figure 4c). Excitation spectra obtained from the fluorescence emission presented in Figure 3 indicate a quite similar absorption profile to those observed in the UV-Vis spectra (Figures S35–S40). Moreover, using 650 nm and 750 nm as the observation

wavelengths, it can be observed that the higher intensities are located around 600 nm, as expected. In contrast, the excitation spectra from Figure 4b present a magnification of the signal located around 700 nm, if compared to the UV-Vis (Figure 2b). This behavior was also expected, indicating that the main fluorescence emission observed at 725 nm is really due to the species with absorption around 700 nm, which is different from the species absorbing between 581 and 611 nm.

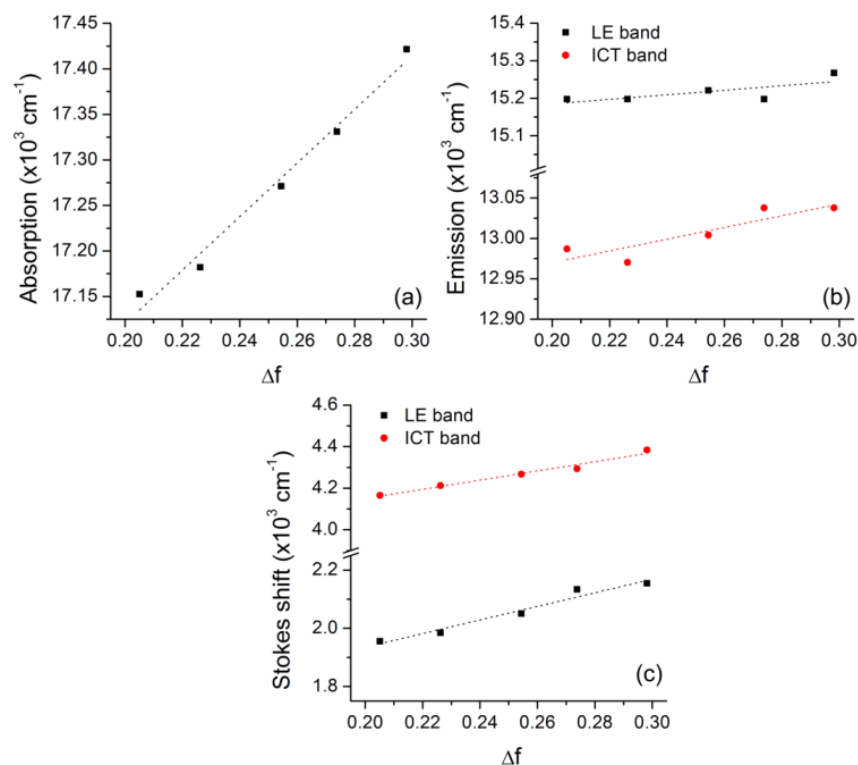


Figure 4. Solvent effect on the spectral position of the (a) absorption, (b) fluorescence emission maxima at LE and ICT bands, and respective (c) Stokes shift for cyanine dye **8b** in different acetonitrile/1,4-dioxane mixtures.

3.3. Theoretical Calculations

Cyanine dyes **6a** and **8a**, chosen as models for the theoretical investigation, have a large chemical space composed, respectively, of 201 and 33 unique conformers. Structure **6a** has the lowest conformer appearing at 38.6% of the Boltzmann population separated from the second lowest conformer (8.0% of the Boltzmann population) by 0.010 kcal·mol⁻¹. Similarly, the Boltzmann distributions indicate that the most stable conformer for cyanine **8a** corresponds to 36.13% of the population, separated from the second lowest conformer (1.9% of the Boltzmann population) by 0.047 kcal·mol⁻¹ (Figure 5).

The selected lower conformers underwent geometric optimizations to the ground and first excited states using Density Functional Theory on the B97-3c scheme. All optimizations accounted for relaxed solvation effects and the ground states are confirmed to be true energy minima by the absence of imaginary vibrational modes. The final ground state geometries showed small distortions due to solvent effects. Cyanine dye **6a** showed small distortions after optimizations with acetonitrile, dichloromethane, and methanol with an average RMSD of 0.007 Å. Similarly, cyanine **8a** after being optimized under acetonitrile, dichloromethane, ethyl acetate, and methanol differs by an average RMSD of only 0.23 Å from each other. As expected, differences between ground and first excited state geometries are small (Figure S41), as electronic absorption occurs extremely fast [62]. As can be seen in Figures S42 and S43, the change in the solvation environment also has just a small effect on the HOMO-LUMO gap described by Density Functional Theory, leading to variations in the order of milihartrees. An additional investigation based on the CHarges from

Electrostatic Potentials using a Grid-based method (CHELPG) [64] showed, also, that the solvation environment itself has little to no impact on atomic charge distribution. A standard deviation (σ) of 0.001 charge units for **6a** and 0.003 charge units for cyanine dye **8a** was obtained after comparing the implicit solvation models by Density Functional Theory, as can be seen in data available in Tables S2 and S3. After confirming that solvation effects have only small impacts on geometric and electronic configurations, our analysis of ground and excited state geometries was based on a higher computational level based on Orbital-Optimized, Spin-Component Scaled Second Order Many-Body Perturbation Theory (OO-SCS-MP2) to avoid restrictions imposed by the Koopmans theorem on Density Functional Theory [65,66]. The HOMO-LUMO gap observed for cyanine dye **8a** on the ground state is 6.57 eV with a slight reduction in the excited state configuration to a gap of 6.42 eV. Charge transfer seems to be extremely relevant during the GS-ES transition due to an observed increase in dipole moment measured by the relaxed MP2 electronic density, going from 2.93 to 3.14 Debye, a 7% increase with noticeable dipole vector repositioning (Figure 6). The same trend is observed for cyanine precursor **6a**, but with a remarkable increase of 27.32%, from 1.83 to 2.33 Debye; the orientation of the total dipole moment vector is, also, drastically changed, as can be seen in Figure 6, indicating a relevant charge transfer effect between GS and ES.

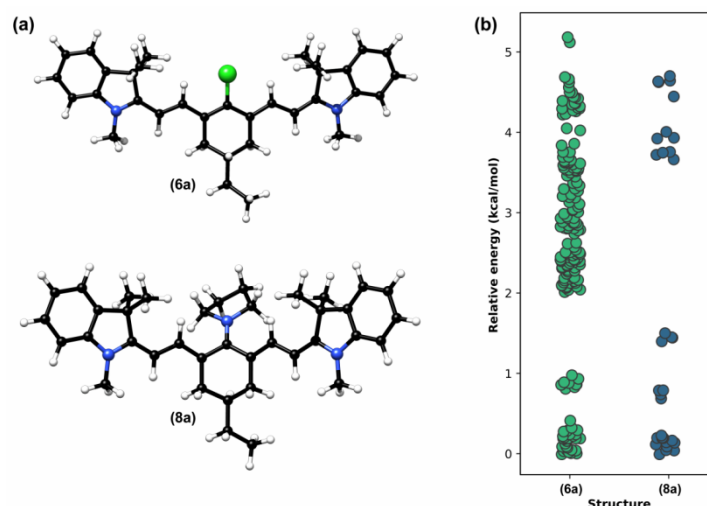


Figure 5. (a) Lowest and more stable conformers for cyanine dyes **6a** and **8a**, and (b) relative energy distribution of every unique conformer on its respective chemical space.

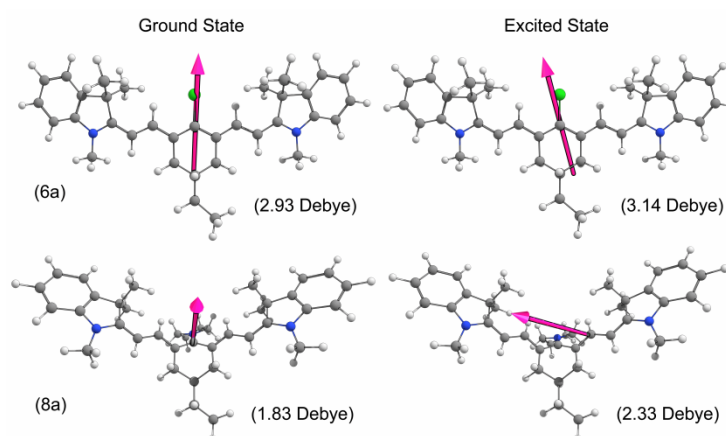


Figure 6. Change in dipole moment between ground and excited state of cyanine dyes **6a** (top) and **8a** (bottom).

Our analysis using the Molecular Electrostatic Potential Surface (MEPS) reveals that both molecules have a higher concentration of negative charge (represented in red) toward the center (Figure S44), while the indoline “wings” remain, overall, positively charged. Upon transition to the first excited state, the *meso*-substituted heptamethine cyanine dye **8a** migrates a considerable amount of negative charge to the center-left side of the molecule, in the opposite direction of the ethyl “tail”. Charge transfer visualization using MEPS is not as straightforward for cyanine dye **6a**, because the dipole moment change is also due to a greater geometric change on the excited state and not just due to an almost vertical ground-to-excited transition as expected on cyanine **8a**. It is still possible to discern a slight increase in negative charge toward the upper center of the molecule as the wings become more positive. The Configuration Interaction Singles (CIS) calculated for both cyanines corroborates that only the immediate frontier orbitals are substantially involved in the first electronic transition with an 89% HOMO-LUMO character for cyanine **8a** and 86% HOMO-LUMO character for cyanine **6a**. The Electronic Density Difference (EDD) [67] was used as a tool to describe the dynamic vertical charge transfer between the frontier orbitals by exploring the hole–particle formalism (Figure 7a). It could also be observed that, to some extent, conjugation plays an important role in the ground state of the molecules and their first excited state (Figure 7b). Applying the Pipek–Mezey localization method [68,69], it was possible to quantify the bonds with high delocalization character. Cyanine dye **6a** accounts for a significantly higher delocalized orbital composition, presenting 10 bonds with a small electronic population. On the other hand, cyanine dye **8a** presents only 6 delocalized orbitals, probably due to not being as planar as dye **6a** and reducing the conjugation effects.

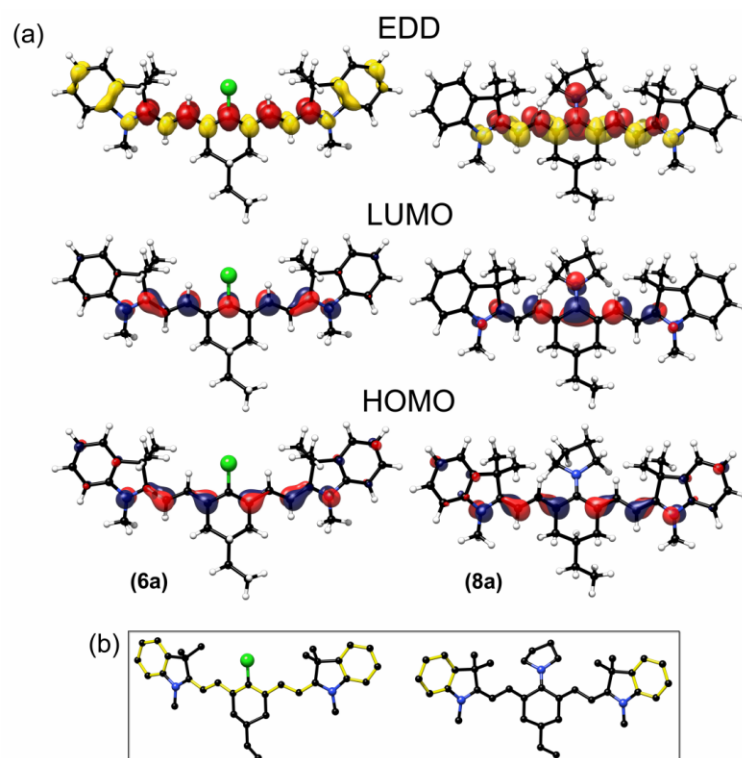


Figure 7. (a) Electronic Density Difference (EDD) with isosurface = 0.0016 for cyanine dyes **6a** and **8a**. The red color indicates a vertical charge increase and the yellow indicates a vertical charge decrease for the GS-ES transition. HOMO and LUMO orbitals have isosurface = 0.05 with the (+) phase color coded as red and the (−) phase as blue. (b) Bonds with strong delocalized character (yellow) calculated by the Pipek–Mezey method. Hydrogens were omitted for clarity.

3.4. Bioimaging

It was observed that all studied *meso*-substituted cyanines kept their optical properties in the dark at room temperature for over 4 weeks, presenting UV-Vis and PL spectra

with similar intensity and shape. It was reported that traditional cyanine dyes display poor photostability [16,70,71]; however, it was observed that the incorporation of a rigid cyclohexenyl ring in the polymethine chain leads to increased photostability [72]. In addition, it was also reported that an improved photostability on the cyanine scaffold takes place upon the incorporation of electron-withdrawing groups [73]. Based on these results, and the studies regarding very close structures with their respective photostability studies [71,73], it was decided to investigate their ability in cell staining without a previous photostability experiment, as usually presented in the literature [42,73]. In this sense, their ability to stain cellular compartments in fixed and live cells was explored (Figures 8 and 9). As shown in Figure 8, cyanine dye **8a**, used as a model, showed strong staining of cellular cytoplasm with long-lasting staining, remaining 24 h after the incubation in fixed cells. Similarly, the cyanine could also stain the cellular cytoplasm of live cells (Figure 9). It was also verified whether this cyanine could compromise cell adhesion (Figure 10), where there is no impairment of cell adhesion. These results demonstrated that cyanine dye **8a** could be used as a fluorescent probe in biotechnology and, more specifically, in protocols of cytochemistry for cytoplasm labeling. Further investigations are in progress for specific staining of selected organelles.

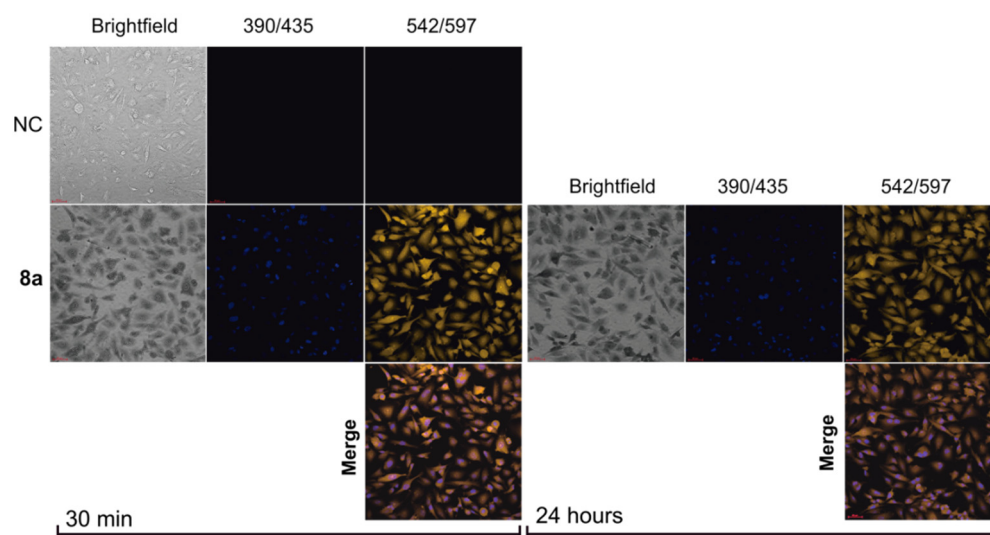


Figure 8. Fluorescent staining of fixed (paraformaldehyde 4%) cells using the *meso*-substituted cyanine **8a** (5 μ M). The first column shows the brightfield, the central column shows the fluorescence of cells incubated with the nuclear dye Hoescht, and the third column shows cyanine **8a**. The result after 30 min of incubation is shown on the left, and that after 24 h of incubation is shown on the right. The first line represents cells without dye (negative control) and the third line represents the merge of Hoescht and cyanine **8a**. Scale bar (red) = 60 μ m.

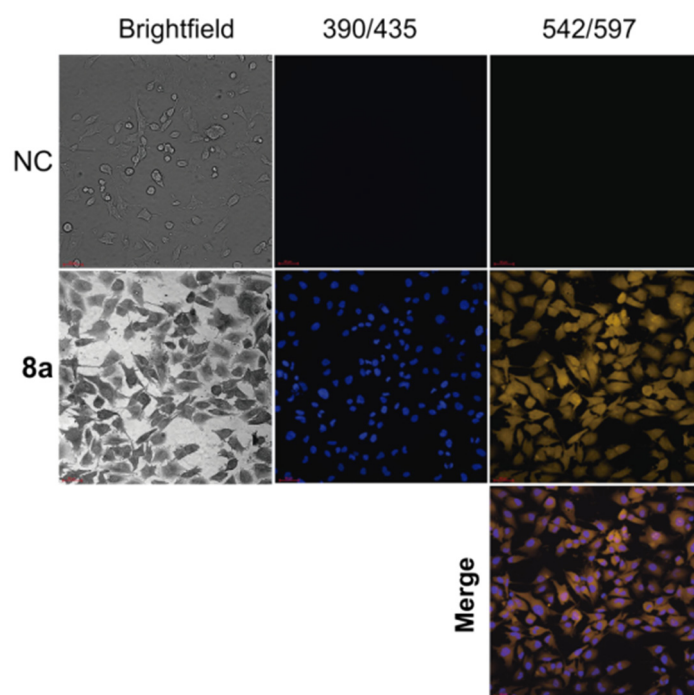


Figure 9. Fluorescent staining of live cells using the *meso*-substituted cyanine **8a** ($5\ \mu\text{M}$). The images were obtained 30 min after incubation. NC = control. The first column shows the brightfield, the central column shows the fluorescence of cells incubated with the nuclear dye Hoescht, and the third column shows cyanine **8a**. The first line represents cells without dye (negative control), the second line represents cells exposed to cyanine **8a**, and the third line represents the merge of Hoescht and cyanine **8a**. Scale bar (red) = $60\ \mu\text{m}$.

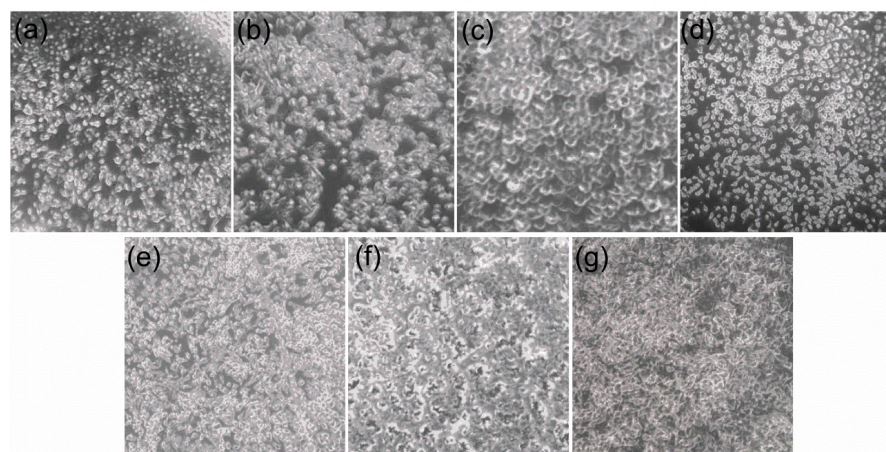


Figure 10. Optical images of cellular confluence after treatment of increasing doses of cyanine dye **8a**: (a) negative control, (b) $0.005\ \mu\text{M}$, (c) $0.01\ \mu\text{M}$, (d) $0.05\ \mu\text{M}$, (e) $0.1\ \mu\text{M}$, (f) $0.5\ \mu\text{M}$, and (g) $5.0\ \mu\text{M}$ after 30 min of incubation.

4. Conclusions

Chlorine heptamethine cyanine dyes were obtained in good yields using a methodology between quaternary indoles and a pentamethine salt, minimizing photooxidation. These cyanines presented a simple and behaved photophysical behavior with no evidence of aggregation in both ground and excited states. In a second step, they were used as molecular scaffolds to synthesize *meso*-substituted derivatives by reaction with pyrrolidine via the $S_{\text{RN}}1$ mechanism with good yields. In this case, the substitution at the *meso* position showed a fundamental role in their photophysics, presenting intricate behavior but still

related to monomeric species. DFT calculations showed that solvation effects, despite being present, are not responsible for relevant geometric or electronic changes on the studied cyanine dyes. Charge transfers between the ground and first excited states are responsible for an increase in negative charge to the center of the molecule, while the external rings become more positive. It is also clear that conjugation effects are much more active on the *meso*-substituted heptamethine cyanine dye due to its greater planarity in comparison to its chlorine heptamethine cyanine dye precursor. Finally, the observed photophysical features of the *meso*-substituted heptamethine cyanines were successfully used to explore their application as fluorescent probes in biological media, showing potential for cytoplasm labeling.

Supplementary Materials: The Supplementary Materials are available online at <https://www.mdpi.com/article/10.3390/chemosensors11010047/s1>. Figures S1–S20 (original spectra from the spectroscopic characterization), Figures S21–S40 and Table S1 (additional photophysical data), and Figures S41–S44, and Tables S2 and S3 (additional theoretical data).

Author Contributions: Conceptualization, F.S.R., D.J.M., H.d.C.S.J. and R.d.C.D.; methodology, R.d.C.D., H.d.C.S.J., D.J.M. and F.d.S.S.; validation, F.S.R. and D.J.M.; investigation, D.d.S.F., A.M.M., L.K.R., F.d.S.S., H.d.C.S.J. and R.d.C.D.; resources, F.S.R. and D.J.M.; writing—original draft preparation, F.S.R., D.J.M. and H.d.C.S.J.; writing—review and editing, R.d.C.D., H.d.C.S.J., D.J.M. and F.S.R.; visualization, F.S.R.; supervision, F.S.R. and D.J.M.; project administration, F.S.R.; funding acquisition, F.S.R. and D.J.M. All authors have read and agreed to the published version of the manuscript.

Funding: This research was funded by Fundação de Amparo à Pesquisa do Estado do Rio Grande do Sul (FAPERGS), grant number 17/2551-0000968-1; National Council for Scientific and Technological Development (CNPq), grant number 409855/2018-9 and 305954/2019-9 and Coordenação de Aperfeiçoamento de Pessoal de Nível Superior (CAPES), Finance Code 001.

Institutional Review Board Statement: Not applicable.

Informed Consent Statement: Not applicable.

Data Availability Statement: Not applicable.

Acknowledgments: All theoretical calculations were performed using the Lobo Carneiro supercomputer from Núcleo Avançado de Computação de Alto Desempenho (NACAD), under Project ID a20006e.

Conflicts of Interest: The authors declare no conflict of interest.

References

1. Reichardt, C. Chiral polymethine dyes: A remarkable but forgotten conjugated π system. *J. Phys. Org. Chem.* **1995**, *8*, 761–773. [[CrossRef](#)]
2. Panigrahi, M.; Dash, S.; Patel, S.; Mishra, B.K. Syntheses of cyanines: A review. *Tetrahedron* **2012**, *68*, 781–805. [[CrossRef](#)]
3. Bricks, J.L.; Kachkovskii, A.D.; Slominskii, Y.L.; Gerasov, A.O.; Popov, S.V. Molecular design of near infrared polymethine dyes: A review. *Dyes Pigm.* **2015**, *121*, 238–255. [[CrossRef](#)]
4. Shindy, H.A. Fundamentals in the chemistry of cyanine dyes: A review. *Dyes Pigm.* **2017**, *145*, 505–513. [[CrossRef](#)]
5. Bouit, P.A.; Aronica, C.; Toupet, L.; Le Guennic, B.; Andraud, C.; Maury, O. Continuous symmetry breaking induced by ion pairing effect in heptamethine cyanine dyes: Beyond the cyanine limit. *J. Am. Chem. Soc.* **2010**, *132*, 4328–4335. [[CrossRef](#)]
6. Strehmel, B.; Schmitz, C.; Kütahya, C.; Pang, Y.; Drewitz, A.; Mustroph, H. Photophysics and photochemistry of NIR absorbers derived from cyanines: Key to new technologies based on chemistry. *Beilstein J. Org. Chem.* **2020**, *16*, 415–444. [[CrossRef](#)]
7. Štacková, L.; Muchová, E.; Russo, M.; Slavíček, P.; Štacko, P.; Klán, P. Deciphering the structure-property relations in substituted heptamethine cyanines. *J. Org. Chem.* **2020**, *85*, 9776–9790. [[CrossRef](#)]
8. Usama, S.M.; Thompson, T.; Burgess, K. Productive manipulation of cyanine dye π -networks. *Angew. Chem. Int. Ed.* **2019**, *8*, 8974–8976. [[CrossRef](#)]
9. Exner, R.M.; Cortezon-Tamarit, F.; Pascu, S.I. Explorations into the effect of *meso*-substituents in tricarbocyanine dyes: A path to diverse biomolecular probes and materials. *Angew. Chem. Int. Ed.* **2020**, *60*, 6230–6241. [[CrossRef](#)]
10. Pascal, S.; Haefele, A.; Monnereau, C.; Charaf-Eddin, A.; Jacquemin, D.; Le Guennic, B.; Andraud, C.; Maury, O. Expanding the polymethine paradigm: Evidence for the contribution of a bis-dipolar electronic structure. *J. Phys. Chem. A* **2014**, *118*, 4038–4047. [[CrossRef](#)]
11. Zhang, J.; Moemeni, M.; Yang, C.; Liang, F.; Peng, W.T.; Levine, B.G.; Lunt, R.R.; Borhan, B. General strategy for tuning the Stokes shifts of near infrared cyanine dyes. *J. Mater. Chem. C* **2020**, *8*, 16769–16773. [[CrossRef](#)]

12. Sissa, C.; Painelli, A.; Terenziani, F.; Trotta, M.; Ragni, R. About the origin of the large Stokes shift in aminoalkyl substituted heptamethine cyanine dyes. *Phys. Chem. Chem. Phys.* **2020**, *22*, 129–135. [[CrossRef](#)]
13. Gragg, J.L. Synthesis of Near-Infrared Heptamethine Cyanine Dyes. Ph.D. Thesis, Georgia State University, Atlanta, GA, USA, 2010.
14. Gorka, A.P.; Nani, R.R.; Schnermann, M.J. Cyanine polyene reactivity: Scope and biomedical applications. *Org. Biomol. Chem.* **2015**, *13*, 7584–7598. [[CrossRef](#)] [[PubMed](#)]
15. Dimer, L.M.Z.; Machado, V.G. Chromogenic and fluorogenic chemosensors for detection of anionic analites. *Química Nova* **2008**, *31*, 2134–2146. [[CrossRef](#)]
16. Sun, W.; Guo, S.; Hu, C.; Fan, J.; Peng, X. Recent Development of chemosensors based on cyanine platforms. *Chem. Rev.* **2016**, *116*, 7768–7817. [[CrossRef](#)] [[PubMed](#)]
17. Reichardt, C. Pyridinium-N-phenolate betaine dyes as empirical indicators of solvent polarity: Some new findings. *Pure Appl. Chem.* **2008**, *80*, 1415–1432. [[CrossRef](#)]
18. Peng, X.; Song, F.; Lu, E.; Wang, Y.; Zhou, W.; Fan, J.; Gao, Y. Heptamethine cyanine dyes with a large Stokes shift and strong fluorescence: A paradigm for excited-state intramolecular charge transfer. *J. Am. Chem. Soc.* **2005**, *127*, 4170–4171. [[CrossRef](#)]
19. Machado, V.G.; Nascimento, M.G.; Rezende, M.C. The halochromism of the 1-methyl-8-oxyquinolinium dye. *Spectrosc. Lett.* **1998**, *31*, 359–367. [[CrossRef](#)]
20. Tada, E.B.; Novaki, L.P.; El Seoud, O.A. Solvatochromism in cationic micellar solutions: Effects of the molecular structures of the solvatochromic probe and the surfactant headgroup. *Langmuir* **2001**, *17*, 652–658. [[CrossRef](#)]
21. Keum, S.R.; Roh, S.J.; Ahn, S.M.; Lim, S.S.; Kim, S.H.; Koh, K. Solvatochromic behavior of non-activated indolinobenzospiropyran 6-carboxylates in aqueous binary solvent mixtures. Part II. *Dyes Pigm.* **2007**, *74*, 343–347. [[CrossRef](#)]
22. Medeiros, N.G.; Braga, C.A.; Câmara, V.C.; Duarte, R.C.; Rodembusch, F.S. Near-Infrared fluorophores based on heptamethine cyanine dyes: From their synthesis and photophysical properties to recent optical sensing and bioimaging applications. *Asian J. Org. Chem.* **2022**, *11*, 118–149. [[CrossRef](#)]
23. Thomas, R.G.; Jeong, Y.Y. NIRF heptamethine cyanine dye nanocomplexes for multi modal theragnosis of tumors. *Chonnam Med. J.* **2017**, *53*, 83–94. [[CrossRef](#)]
24. Cosco, E.D.; Spearman, A.L.; Ramakrishnan, S.; Lingg, J.G.; Saccomano, M.; Pengshung, M.; Arús, B.A.; Wong, K.C.; Glasl, S.; Ntziachristos, V.; et al. Shortwave infrared polymethine fluorophores matched to excitation lasers enable non-invasive, multicolour in vivo imaging in real time. *Nat. Chem.* **2020**, *12*, 1123–1130. [[CrossRef](#)]
25. Yang, X.; Shi, C.; Tong, R.; Qian, W.; Zhau, H.E.; Wang, R.; Zhu, G.; Cheng, J.; Yang, V.W.; Cheng, T.; et al. Near IR heptamethine cyanine dye-mediated cancer imaging. *Clin. Cancer Res.* **2010**, *16*, 2833–2844. [[CrossRef](#)]
26. Myochin, T.; Kiyose, K.; Hanaoka, K.; Kojima, H.; Terai, T.; Nagano, T. Rational design of ratiometric near-infrared fluorescent pH probes with various pKa values, based on aminocyanine. *J. Am. Chem. Soc.* **2011**, *133*, 3401–3409. [[CrossRef](#)]
27. Duarte, R.C.; Reimann, L.K.; Rodembusch, F.S.; Duarte, L.G.T.A. 1-Butyl-2,3,3-trimethylindol-1-ium iodide. *IUCrData* **2018**, *3*, x181130. [[CrossRef](#)]
28. Menéndez, G.O.; Pichel, M.E.; Spagnuolo, C.C.; Jares-Erijman, E.A. NIR fluorescent biotinylated cyanine dye: Optical properties and combination with quantum dots as a potential sensing device. *Photochem. Photobiol. Sci.* **2013**, *12*, 236–240. [[CrossRef](#)]
29. Neese, F.; Wennmohs, F.; Becker, U.; Riplinger, C. The ORCA quantum chemistry program package. *J. Chem. Phys.* **2020**, *152*, 224108. [[CrossRef](#)]
30. Pracht, P.; Bohle, F.; Grimme, S. Automated exploration of the low-energy chemical space with fast quantum chemical methods. *Phys. Chem. Chem. Phys.* **2020**, *22*, 7169–7192. [[CrossRef](#)]
31. Bannwarth, C.; Ehlert, S.; Grimme, S. GFN2-XTB—An accurate and broadly parametrized self-consistent tight-binding quantum chemical method with multipole electrostatics and density-dependent dispersion contributions. *J. Chem. Theory Comput.* **2019**, *15*, 1652–1671. [[CrossRef](#)]
32. Brandenburg, J.G.; Bannwarth, C.; Hansen, A.; Grimme, S. B97-3c: A revised low-cost variant of the B97-D density functional method. *J. Chem. Phys.* **2018**, *148*, 064104. [[CrossRef](#)] [[PubMed](#)]
33. Becke, A.D. Density-functional thermochemistry. V. Systematic optimization of exchange-correlation functionals. *J. Chem. Phys.* **1997**, *107*, 8554–8560. [[CrossRef](#)]
34. Weigend, F.; Ahlrichs, R. Balanced basis sets of split valence, triple zeta valence and quadruple zeta valence quality for H to Rn: Design and assessment of accuracy. *Phys. Chem. Chem. Phys.* **2005**, *7*, 3297–3305. [[CrossRef](#)] [[PubMed](#)]
35. Grimme, S.; Antony, J.; Ehrlich, S.; Krieg, H. A consistent and accurate ab initio parametrization of density functional dispersion correction (DFT-D) for the 94 elements H-Pu. *J. Chem. Phys.* **2010**, *132*, 154104. [[CrossRef](#)] [[PubMed](#)]
36. Sure, R.; Grimme, S. Corrected small basis set Hartree-Fock method for large systems. *J. Comput. Chem.* **2013**, *34*, 1672–1685. [[CrossRef](#)]
37. Cammi, R.; Mennucci, B.; Tomasi, J. Fast evaluation of geometries and properties of excited molecules in solution: A Tamm-Dancoff model with application to 4-dimethylaminobenzonitrile. *J. Phys. Chem. A* **2000**, *104*, 5631–5637. [[CrossRef](#)]
38. Neese, F.; Schwabe, T.; Kossmann, S.; Schirmer, B.; Grimme, S. Assessment of orbital-optimized, spin-component scaled second-order many-body perturbation theory for thermochemistry and kinetics. *J. Chem. Theory Comput.* **2009**, *5*, 3060–3073. [[CrossRef](#)]

39. Dost, T.L.; Gressel, M.T.; Henary, M. Synthesis and optical properties of pentamethine cyanine dyes with carboxylic acid moieties. *Anal. Chem. Insights* **2017**, *12*, 1–6. [[CrossRef](#)]
40. Shi, Q.Q.; Sun, R.; Ge, F.J.; Xu, Q.F.; Li, N.J.; Lu, J.M. A comparative study of symmetrical and unsymmetrical trimethine cyanine dyes bearing benzoxazolyl and benzothiazolyl groups. *Dyes Pigm.* **2012**, *93*, 1506–1511. [[CrossRef](#)]
41. Chapman, G.; Henary, M.; Patonay, G. The effect of varying short-chain alkyl substitution on the molar absorptivity and quantum yield of cyanine dyes. *Anal. Chem. Insights* **2011**, *6*, 29–36. [[CrossRef](#)]
42. Shershov, V.E.; Spitsyn, M.A.; Kuznetsova, V.E.; Timofeev, E.N.; Ivashkina, O.A.; Abramov, I.S.; Nasedkina, T.V.; Zasedatelev, A.S.; Chudinov, A.V. Near-infrared heptamethine cyanine dyes. Synthesis, spectroscopic characterization, thermal properties and photostability. *Dyes Pigm.* **2013**, *97*, 353–360. [[CrossRef](#)]
43. Owens, E.A.; Bruschi, N.; Tawney, J.G.; Henary, M. A microwave-assisted and environmentally benign approach to the synthesis of near-infrared fluorescent pentamethine cyanine dyes. *Dyes Pigm.* **2015**, *113*, 27–37. [[CrossRef](#)]
44. Salon, J.; Wolinska, E.; Raszkievicz, A.; Patonay, G.; Strekowski, L. Synthesis of benz[e]indolium heptamethine cyanines containing C-substituents at the central portion of the heptamethine moiety. *J. Heterocycl. Chem.* **2005**, *42*, 959–961. [[CrossRef](#)]
45. Pascal, S.; Chi, S.H.; Perry, J.W.; Andraud, C.; Maury, O. Impact of ion-pairing effects on linear and nonlinear photophysical properties of polymethine dyes. *ChemPhysChem* **2020**, *21*, 2536–2542. [[CrossRef](#)]
46. Strickler, S.J.; Berg, R.A. Relationship between absorption intensity and fluorescence lifetime of molecules. *J. Chem. Phys.* **1962**, *37*, 814–822. [[CrossRef](#)]
47. Turro, N.J.; Scaiano, J.C.; Ramamurthy, V. *Principles of Molecular Photochemistry: An Introduction*, 1st ed.; University Science Book: Sausalito, CA, USA, 2008.
48. Yao, Y.; Liang, Y.; Shrotriya, V.; Xiao, S.; Yu, L.; Yang, Y. Plastic near-infrared photodetectors utilizing low band gap polymer. *Adv. Mater.* **2007**, *19*, 3979–3983. [[CrossRef](#)]
49. Qian, G.; Zhong, Z.; Luo, M.; Yu, D.; Zhang, Z.; Wang, Z.Y.; Ma, D. Simple and efficient near-infrared organic chromophores for light-emitting diodes with single electroluminescent emission above 1000 nm. *Adv. Mater.* **2009**, *21*, 111–116. [[CrossRef](#)]
50. Shapiro, B.I. Molecular assemblies of polymethine dyes. *Russ. Chem. Rev.* **2006**, *75*, 433–456. [[CrossRef](#)]
51. Lee, H.; Mason, J.C.; Achilefu, S. Synthesis and spectral properties of near-infrared aminophenyl-, hydroxyphenyl-, and phenyl-substituted heptamethinecyanines. *J. Org. Chem.* **2008**, *3*, 723–725. [[CrossRef](#)]
52. Pydzińska, K.; Ziótek, M. Solar cells sensitized with near-infrared absorbing dye: Problems with sunlight conversion efficiency revealed in ultrafast laser spectroscopy studies. *Dyes Pigm.* **2015**, *122*, 272–279. [[CrossRef](#)]
53. Arjona-Esteban, A.; Stolte, M.; Würthner, F. Conformational switching of π -conjugated junctions from merocyanine to cyanine states by solvent polarity. *Angew. Chem. Int. Ed.* **2016**, *55*, 2470–2473. [[CrossRef](#)]
54. Egorov, V.V. Nature of the optical band shapes in polymethine dyes and H-aggregates: Dozy chaos and excitons. Comparison with dimers, H^{*}- and J-aggregates. *R. Soc. Open Sci.* **2017**, *4*, 160550. [[CrossRef](#)]
55. Bricks, J.L.; Slominskii, Y.L.; Panas, I.D.; Demchenko, A.P. Fluorescent J-aggregates of cyanine dyes: Basic research and applications review. *Methods Appl. Fluoresc.* **2018**, *6*, 012001. [[CrossRef](#)]
56. Eisfeld, A.; Briggs, J. The shape of the J-band of pseudoisocyanine. *Chem. Phys. Lett.* **2007**, *446*, 354–358. [[CrossRef](#)]
57. Würthner, F.; Kaiser, T.E.; Saha-Möller, C.R. J-aggregates: From serendipitous discovery to supramolecular engineering of functional dye materials. *Angew. Chem. Int. Ed.* **2011**, *50*, 3376–3410. [[CrossRef](#)]
58. Rösch, U.; Yao, S.; Wortmann, R.; Würthner, F. Fluorescent H-aggregates of merocyanine dyes. *Angew. Chem. Int. Ed.* **2006**, *45*, 7026–7030. [[CrossRef](#)]
59. El-Daly, S.A.; Asiri, A.M.; Alamry, K.A. Experimental determination of ground and excited state dipole moments of *N,N*-bis(2,5-di-tert-butylphenyl)-3,4:9,10-perylenebis(dicarboximide) (DBPI) a photostable laser dye. *J. Fluoresc.* **2014**, *24*, 1307–1311. [[CrossRef](#)]
60. Lippert, E.; Lüder, W.; Moll, F.; Nägele, W.; Boos, H.; Prigge, H.; Seibold-Blankenstein, I. Umwandlung von elektronenanregungsenergie. *Angew. Chem.* **1961**, *73*, 695–706. [[CrossRef](#)]
61. Dahiya, P.; Choudhury, S.D.; Maity, D.K.; Mukherjee, T.; Pal, H. Solvent polarity induced structural changes in 2,6-diamino-9,10-anthraquinone dye. *Spectrochim. Acta A* **2008**, *69*, 134–141. [[CrossRef](#)]
62. Lakowicz, J.R. *Principles of Fluorescence Spectroscopy*, 3rd ed.; Springer: New York, NY, USA, 2006.
63. Gündüz, M.G.; da Silva, C.B.; Zanutto, G.M.; Toldo, J.M.; Şimşek, R.; Şafak, C.; Gonçalves, P.F.B.; Rodembusch, F.S. Theoretical and experimental study of the ground and excited states of 1,4-dihydropyridine based hexahydroquinoline derivatives achieved by microwave irradiation. *New J. Chem.* **2017**, *41*, 11686–11694. [[CrossRef](#)]
64. Breneman, C.M.; Wiberg, K.B. Determining atom-centered monopoles from molecular electrostatic potentials. The need for high sampling density in formamide conformational analysis. *J. Comput. Chem.* **1990**, *11*, 361–373. [[CrossRef](#)]
65. Stowasser, R.; Hoffmann, R. What do the Kohn-Sham orbitals and eigenvalues mean? *J. Am. Chem. Soc.* **1999**, *121*, 3414–3420. [[CrossRef](#)]
66. Tsuneda, T.; Song, J.W.; Suzuki, S.; Hirao, K. On Koopmans' theorem in density functional theory. *J. Chem. Phys.* **2010**, *133*, 174101. [[CrossRef](#)]
67. Harrison, J.F. On the role of the electron density difference in the interpretation of molecular properties. *J. Chem. Phys.* **2003**, *119*, 8763–8764. [[CrossRef](#)]

68. Pipek, J.; Mezey, P.G. A fast intrinsic localization procedure applicable for ab initio and semiempirical linear combination of atomic orbital wave functions. *J. Chem. Phys.* **1989**, *90*, 4916–4926. [[CrossRef](#)]
69. Høyvik, I.M.; Jansik, B.; Jørgensen, P. Pipek-Mezey localization of occupied and virtual orbitals. *J. Comput. Chem.* **2013**, *34*, 1456–1462. [[CrossRef](#)]
70. Shi, C.; Wu, J.B.; Pan, D. Review on near-infrared heptamethine cyanine dyes as theranostic agents for tumor imaging, targeting, and photodynamic therapy. *J. Biomed. Opt.* **2016**, *21*, 050901. [[CrossRef](#)]
71. Usama, S.M.; Thavornpradit, S.; Burgess, K. Optimized heptamethinecyanines for photodynamic therapy. *ACS Appl. BioMater.* **2018**, *1*, 1195–1205. [[CrossRef](#)]
72. Lee, H.; Mason, J.C.; Achilefu, S. Heptamethine cyanine dyes with a robust C-C bond at the central position of the chromophore. *J. Org. Chem.* **2006**, *71*, 7862–7865. [[CrossRef](#)]
73. Samanta, A.; Vendrell, M.; Das, R.; Chang, Y.T. Development of photostable near-infrared cyanine dyes. *Chem. Commun.* **2010**, *46*, 7406–7408. [[CrossRef](#)]

Disclaimer/Publisher’s Note: The statements, opinions and data contained in all publications are solely those of the individual author(s) and contributor(s) and not of MDPI and/or the editor(s). MDPI and/or the editor(s) disclaim responsibility for any injury to people or property resulting from any ideas, methods, instructions or products referred to in the content.